Bull. Astr. Soc. India (2002) 30, 871–879

The Distribution of the Quiet Sun Photospheric Magnetic Flux

R. Srikanth[1]*, Jagdev Singh[2] and S. P. Bagare[2]
[1]*Center for Theoretical Studies, Indian Institute of Science, Bangalore- 560 012, India.*
[2]*Indian Institute of Astrophysics, Bangalore 34; India.*

Received 27 January 2002; accepted 23 August 2002

Abstract. A gradient-based tessellating algorithm is used to study the magnetic field structure of the quiet Sun photosphere using SoHO full disk magnetograms. We find that the field is not uniformly distributed, but parcelled into flux concentrations. Both the flux and size of the concentrations are found to be described by broad, asymmetric distribution functions. Their mean absolute flux and size are found to be about 1.4×10^{18} mx and 6.1 Mm for both polarities in unsmoothed magnetograms at 5 gauss threshold. These values represent a weighted average for both network- and intranetwork magnetic fields, since the present method cannot currently distinguish between the two regions. Both flux and size distributions become more symmetric and less peaked in response to smoothing of images. Extrapolating this trend to sub-resolution scale, we note a linear decrease in size but a rapid increase in the mean absolute field strength, with asymptotic values of about 400 km and 50 gauss. This exercise shows that the true field strengths of quiet magnetic elements are higher and their size smaller than usually inferred from observations. This is because observation of mixed polarity regions under finite resolution causes the observed flux to be smeared out and apparently modified. Therefore, this flux cannot be interpreted independently of the geometric structure and flux distribution of the concentrations.

Keywords : solar: photosphere – magnetic fields.

*srik@cts.iisc.ernet.in

1. Introduction

The structure of magnetic flux on the solar surface is the result of the interaction of magnetic fields with the convective flows. We find that the magnetic flux is not uniformly distributed, but, even at the scale of a few arcsecs, parcelled into flux concentrations with flux of the order of 10^{18} mx. As a result of buffetting by granules, shear in the flow in which the concentrations are embedded, these concentrations constantly evolve by colliding, merging, cancelling and fragmenting (Martin 1990). The distribution of flux in concentrations is the resultant of these processes, and can hence shed light on them. Here we describe the results of a tessellation-based image processing method to study flux concentrations statistically, and to probe their properties at sub-resolution levels.

2. Data Analysis

The data consists of full disk magnetograms from the Solar and Heliospheric Observatory (SoHO) Michelson Doppler Imager (MDI) covering the period 28–29, June 1996 (Scherrer et al. 1995), with a resolution of 2″ per pixel. Since the cadence of the images is quite large (96 min) compared to the expected lifetimes of flux concentrations, we did not time-average the images. A magnetogram is subjected to a procedure whereby it is mapped into a tessellation, i.e., a pattern of surface-filling non-overlapping tiles. This is based on a technique widely used in many astrophysical and solar studies, in computational geometry and in image analysis for pattern recognition and texture analysis (Okabe, Boots and Sugihara 1992). The method as applied here is a generalization of the Voronoi tessellation technique applied earlier to Ca II K filtergrams and SoHO dopplergrams (cf. Srikanth, Singh and Raju 2000, and references therein). Two steps are involved: first, determining suitable local minima and maxima, and second, by collecting the remaining pixels into tiles labelled uniquely by these extrema (Srikanth and Singh 2000).

The 'steepest descent' algorithm is used to locate the local minima. Here one moves along the steepest negative gradient starting from a point until a local minimum is reached. Analogously, the steepest *positive* gradient is chosen to locate the maxima. Since we wish to interpret these extrema as peaks of magnetic flux concentrations, we select only those maxima which are positively valued and minima that are negatively valued. In the second step, we associate exhaustively all other pixels uniquely to the selected extrema as follows: a given positively valued non-extremal pixel is grouped with that positive local maximum to which it tends according to steepest ascent. Analogously, a given negatively valued non-extremal pixel is associated with that negative local minimum to which it tends according to steepest descent.

The result is a tessellation of the magnetogram into positively and negatively valued 'tiles' or 'cells' anchored to and labelled by, respectively, local maxima or minima (Figure 1). The negative and positive flux tiles occupy mutually complementary regions. The tile boundaries are neutral lines where the field changes sign. The tiles are interpreted as

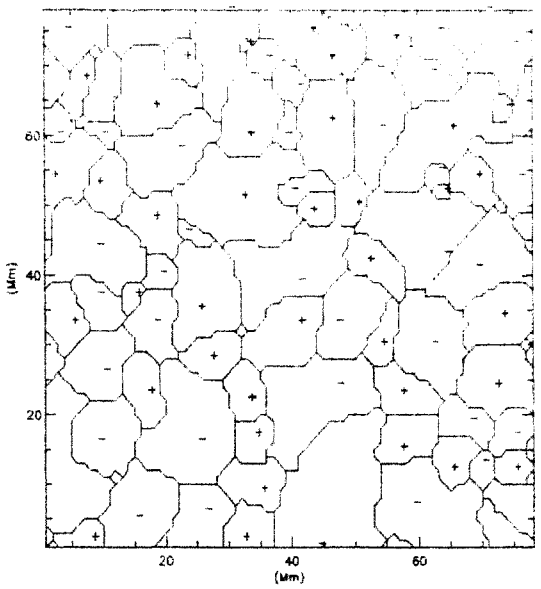

Figure 1. Tessellation of a 80 Mm × 80 Mm magnetogram window smoothed by convolution with a 4″ FWHM gaussian. The '+' and '-' represent, respectively, the extremum of positive and negative tiles.

flux parcels or concentrations. Figure 1 gives us a general idea of how the concentrations are shaped and spatially distributed over a region about 80 Mm × 80 Mm^2 in area. The peak of positive (negative) concentrations is marked by a '+' ('–').

We find that the concentrations are irregularly shaped. There seems to be a clustering of smaller concentrations around some larger ones. The peaks do not necessarily lie at the center-of-mass of the concentrations. In some cases, in fact they lie quite close to the edges.

It might appear at first that the tessellation could be used to sense supergranular boundaries, given that supergranular outflows concentrate relatively large fields at their boundary. However, this is thwarted by the discontinuous and mixed polarity nature of the network flux. The tiles that constitute the tessellation are interpreted as localized regions of same-signed flux at the given effective resolution. At the same time, our resolution is not sufficient to clearly distinguish between network and intra-network tiles, a distinction that would useful, given that these two types are intrinsically different in the true field strength and size (Lin, 1995), and moreover play dissimilar roles in solar atmospheric heating (Sivaraman and Livingston 1982; Kariyappa 1994; Kariappa, Sivaraman and Anandaram 1994). Indeed, even at a resolution as high as 0.″5, the cell wall estimated to be about 5000 km thick, is only about 14 pixels thick. Since the

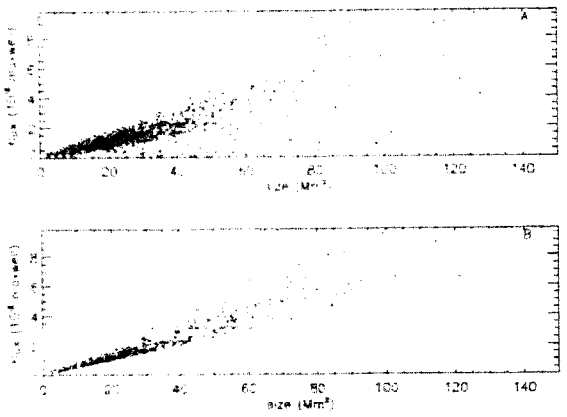

Figure 2. Scatter plot of flux (in units of 10^{18} Mx) against tile size (Mm^2): at zero threshold (panel A), and at 5 gauss threshold (panel B).

present method works best in tessellating broad areas, the inability to distinguish between network and intra-network structres is a current intrinsic limitation of the method.

3. Thresholding the image

Since the images are not time-averaged, it is necessary to boost signal-to-noise (S/N) ratio by other means. Furthermore, the tessellation will sense any undulations, a problem noted in Srikanth, Singh and Raju (2000), not just the desired concentrations. Typically, the undesired tiles will be low flux holders at all sizes. This can be seen in Figure 2. The panel (a) is the result of an unthresholded image tessellation for a region covering seven quiescent windows of size $115'' \times 115''$. The panel (B) is the same data with tiles thresholded at the $B = 5$ gauss level (that is, only tiles with $B \geq 5$ gauss are included).

One effect of thresholding is that it improves the correlation between the fluxes and the areas (Table 1). The correlation improves considerably as we impose a threshold at 5 and 7 gauss levels, which is high enough to avoid noise but low enough not to undersample the flux. The statistics are always similar for both negative and positive tiles, and hence only absolute values are considered throughout this work.

Figure 3 is the flux and size histogram for the tiles from the tessellation of the SoHO magnetograms thresholded at 7 gauss level. In panel (A), we find that the distribution peaks towards lower scales. The results for fluxes and sizes of the tiles for some thresholds in unsmoothed magnetogram tessellation is given in Table 1. The mean size of the tiles, and consquently flux, of the tiles increases with increase in the threshold. The mean

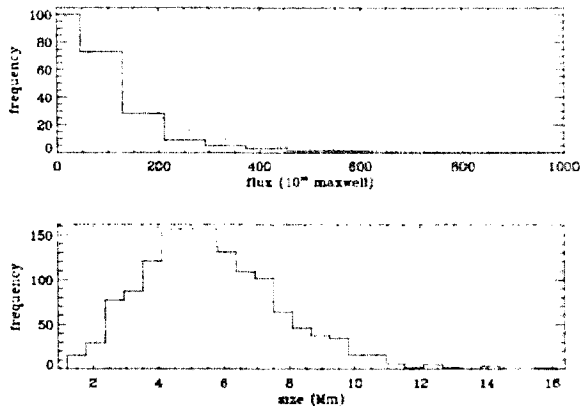

Figure 3. Histogram of flux (panel A) and sizes (panel B) of flux concentrations identified by tessellation at zero smoothing, 5 gauss threshold; the flux distribution is described by an exponential fit with a scale flux of 1.34×10^{18} mx.

field strength at zero thresholding is close to the average quiet region field (for example, LaBonte & Howard (1980) quote a value of 2.2 gauss).

threshold	mean abs. flux (10^{18} mx)	size (Mm)	mean abs. field (gauss)	flux-area correlation
0.0	1.0	5.9	5.4	0.80
5.0	1.4	6.1	6.9	0.91
7.0	2.1	6.8	8.5	0.93

Table 1. Mean absolute tile flux, size and field strength for various thresholds on an unsmoothed SoHO magnetogram. The statistics combines results for positive and negative flux tiles.

The mean size of the tiles at the 5 gauss threshold is 6.1 Mm. Wang (1988) found the autocorrelation size of network elements to be 5.74 Mm. It is also comparable with the width of the network, about 5.5 Mm, quoted by Singh and Bappu (1981). The mean tile absolute flux is found to be 1.4×10^{18} mx, not incompatible with that of Wang et al. (1995). It therefore seems reasonable to identify the tiles with flux concentrations and/or network elements at this threshold. This is further corroborated by autocorrelation of the SoHO magnetograms, which yields sizes around 30 Mm, comparable with traditionally quoted supergranular sizes. However, as noted in Srikanth, Singh and Raju (2000), the resolution dependence of the tile statistics means that there is no simple interpretation of the tiles.

We find that an exponential fit, with a scale flux of 1.34×10^{18} mx, well describes the fall in the distribution function in Figure 3. In Srikanth and Singh (2000), we presented

the distribution of the unthresholded tessellation. A turn-down was observed in the distribution function around 0.64×10^{18} mx, which was attributed to an artefact due to the data noise.

4. Effect of smoothing the magnetograms

The data for the variation of field strength and size of tiles with respect to the smoothing parameter λ is given in Table 2. In view of the discussion in the preceding section, in order to exclude tiles that cannot reasonably be flux concentrations, in the case of $\lambda = 0, 0.72$ Mm, thresholds were set at $B = 5$ gauss. As noted in the case of Ca II K filtergrams and SoHO Dopplergrams (Srikanth, Singh and Raju 2000), smoothing causes an increase in mean size of the tiles. It tends to level out small intensity-fluctuations, which are also of small scale. This results in a faster loss of smaller tiles than in that of larger ones, producing larger mean tile sizes. Simultaneously, smoothing combines opposite signed fluxes, thereby producing lower mean fluxes.

λ (arcsec)	mean abs. field (gauss)	mean size (Mm)
0.0	5.5	5.9
1.0	4.0	6.3
2.0	2.2	7.7
3.0	1.7	10.1
4.0	1.4	12.6
5.0	1.2	14.8

Table 2. Mean absolute tile field strength and mean size as a function of the smoothing parameter λ. The field strength decreases while size increases. The statistics combines results for positive and negative flux tiles.

The dependence of the mean field and mean size on the smoothing means that these parameters will in general depend on the resolution of the magnetogram (Srikanth, Singh and Raju 2000). The value of 5.5 gauss and 5.9 Mm for the tiles obtained at $\lambda = 0$ cannot therefore be thought of as the actual parameters of the concentrations, but the parameter values as modified by the finite resolution of the image.

To overcome this problem, we re-parametrize the field and size in terms of the effective resolution $\rho = \sqrt{\lambda^2 + s^2}$, where $s = 2''.0$ is the seeing. The result of this exercise is given in Figure 4. The upper panel shows that the field strength increases rapidly as ρ decreases, with an accompanying quartic least-squares best fit given by $B = 53.2 - 70.9\rho + 36.4\rho^2 - 8.3\rho^3 + 0.7\rho^4$. This means that the asymptotic absolute mean field strength at the smallest scales is as high as 53 gauss, and possibly higher, in quiet Sun regions. However, in view of the strong curvature and lack of data points at small ρ, other fits might well be possible. Data at higher resolution can be of help.

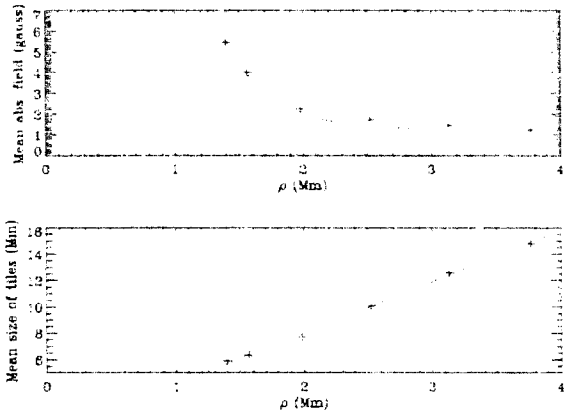

Figure 4. The mean absolute tile field strength (upper panel) and the mean size (lower panel) as a function of the effective resolution parameter ρ. Smoothing combines fluxes of opposite signs, so that greater smoothing produce smaller mean flux. Its effect on size is however to iron out small undulations leading to larger mean tile sizes.

In a later work, we wish to apply the current technique to higher resolution SoHO magnetogram data. On the other hand, the variation of tile size with ρ appears to be almost linear in the available range. We determined the quadratic best fit to be $a = 0.42 + 3.8\rho + 0.02\rho^2$, where a is the mean size in Mm of the tiles.

Assuming that we can extrapolate the curves in Figure 4 to the sub-resolution range, we find that for $\rho = 0$, i.e, at maximum possible resolution, the mean size of the tile is about 420 km. For the asymptotic field value of 50 gauss inferred above, this corresponds to a flux of about 2.5×10^{17} mx. It is interesting that surprisingly strong fields ($\sim$ 500 G) and small magnetic elements ($\sim$ 70 km) are inferred also by Lin (1995) for intranetwork weak magnetic fields.

5. Amplitude of the magnetic field

Some information about how flux is distributed within a concentration can be obtained by studying the flux-size relation. These two variables are strongly related, as evident from Figure 2. As part of the model to describe a tile, we assume that the magnetic flux density in the concentration has a Gaussian profile given by:

$$B = B_0 \exp\left(-r^2/R_0^2\right), \tag{1}$$

where r is the radial coordinate centered on the concentration, and B_0 is the amplitude of the magnetic field. The total flux in a model tile is taken to be

$$\phi \approx 2\pi B_0 \int_0^\infty \exp\left(-r^2/R_0^2\right) r dr = \pi B_0 R_0^2. \tag{2}$$

Although the radius of the concentration is finite, the upper integration limit in Eq. (2) is a valid approximation because the flux falls off rapidly in a Gaussian profile for large r. In Figure 2 (B), from a least squares best fit we find that the flux $\phi \propto S^{1.1}$, where S is area of a tile. In Eq. (2), letting $S \equiv \pi R_0^2$, we find:

$$B_0 \propto S^n, \tag{3}$$

where $n = 0.1$, which suggests that the amplitude of the field increases with the size of the flux concentration.

6. Conclusions

In an earlier work (Srikanth, Singh and Raju 2000), we pointed out that the present method for studying solar surface structure and extracting length-scales requires a careful interpretation, preferably on basis of auxillary criteria. Nevertheless, some qualitative conclusions can be spelt out. One point is that the flux covering the quiet Sun is not uniformly spread out with about 5 gauss mean field strength, but instead parcelled into a patchwork of concentrations of higher field strengths. As deduced from the SoHO full disk magnetograms, these quiet region flux concentrations have a mean size of about 400 km with a mean field strength in excess of 50 gauss that is weakly dependent on the size of the concentrations. As noted in Section II, these values ignore the difference between network and intra-network magnetic fields, and to that extent, may be viewed as a weighted average behaviour of quiet magnetic flux for these two regions.

Further, these values are resolution-dependent. For example, even though the asymptotic size for large extrapolated seeing gave the same behaviour for both Ca II filtergrams (seeing = 3″.4) (Singh et al. 1995) and SoHO time-averaged full disk dopplergrams (seeing = 2″), their asymptotic behaviour for vanishing seeing yielded different size scales (Srikanth, Singh and Raju 2000). An application of the tessellation algorithm to high resolution Swedish Vacuum Solar Telescope Ca II K data (0″.4) confirmed this conclusion (Krishnakumar, Venkatakrishnan and Srikanth 2000). What emerges is that the conventionally quoted quiet Sun field strengths ($\sim$ 5 gauss) probably underestimates the true strength, owing to the smearing out of flux in mixed polarity regions observed with lower spatial resolution.

We thank Dr. P. H. Scherrer and the SoHO consortium for providing us with the MDI/SOI full disk magnetogram data.

References

Kariyappa, R., 1994, *Solar Physics*, **154**, 19.
Kariyappa, R., Sivaraman, K. R. and Anadaram, M. N., 1994, *Sol. Phys.* **151**, 243.
Krishnakumar, V., Venkatakrishnan, P. and Srikanth, R., 2000, Bull. Astr. Soc. India , 28, 23.
LaBonte, B. J. & Howard, R., *Sol. Phys.* **80**, 15 (1980).
Lin, H., 1995, *Astroph. Jl.* **446**, 421.
Martin, S. F. in IAU Symp. 138, *Solar Photosphere: Structure, Convection, and Magnetic Fields*, ed. J. O. Stenflo (Dordrecht, Kluwer) **129** (1990).
Okabe, A., Boots, B., & Sugihara, K. Spatial Tesselations; Concepts and Applications of Voronoi Diagrams (New York, Wiley, 1992)
Scherrer, P. H., R. S. Bogart, R. I. Bush, J. T. Hoeksema, A. G. Kosovichev, J. Schou, W. Rosenberg, L. Springer, T. D. Tarbell, A. Title, C. J. Wolfson, I. Zayer & t. M. E. Team, *Solar Physics*, **162**, 129, 1995.
Singh, J. & Bappu, M. K. V. 1982, Sol. Phys., 71, 161.
Singh, J., Nagabhûshana, Babu, G. S. D., and Uddin, W. 1994 Sol. Phys., 153, 157.
Sivaraman, K. R. and Livingston, W. C., 1982, Sol. Phys. **80** 227.
Srikanth, R., Singh, J., and Raju, K. P., *Astrophys. J.* **534**, 1008 (2000).
Srikanth, R. and Singh, J., 2000, Journal Astron. Astrophys. **21**, 265.
Wang, H., 1988, *Sol. Phys.* **116**, 1.
Wang, J., Wang, H., Tang, F., Lee, J. W., Zirin, H., *Sol. Phys.* **160**, 277 (1995).